Ice-atmosphere interactions during sea-ice advance and retreat in the western Antarctic Peninsula region

S. E. Stammerjohn,[1] M. R. Drinkwater,[2] R. C. Smith,[3] and X. Liu[4]

Received 16 July 2002; revised 4 June 2003; accepted 28 July 2003; published 21 October 2003.

[1] The seasonal evolution of sea-ice extent, concentration, and drift in the western Antarctic Peninsula (WAP) region, along with regional atmospheric synoptic variability, are described for a winter period (1992) when sea-ice advance and retreat were both anomalously early. Daily time series of winds, opening and closing of the sea-ice cover, and volume fluxes in and out of the WAP region indicate that synoptic variability in meridional winds determines whether the ice-edge advances or retreats on daily to weekly timescales. The importance of this finding is that the dynamics, as opposed to the thermodynamics, initiate, and thereby dominate, in the production of ice-edge anomalies. Further, the abrupt mid-winter shift from persistently positive to negative ice-edge anomalies indicates that there was a distinct change in the regional atmospheric circulation. The ice-atmosphere interactions in the winter of 1992 are then compared to those in the winter of 1990, when sea-ice advance and retreat were both late instead of early, but again the mid-winter shift was abrupt. The comparison highlights possible circumpolar and tropical-polar atmospheric linkages in the South Pacific that involve changes in the amplitude/phase of the semi-annual oscillation (SAO), which in turn appear to be related to El Niño-Southern Oscillation (ENSO) changes in the tropical Pacific. The implication of a dynamically driven ice-atmosphere system, together with an intraseasonal ENSO linkage, further supports the idea that the WAP region is particularly sensitive to changes in the tropical Pacific. *INDEX TERMS:* 4207 Oceanography: General: Arctic and Antarctic oceanography; 4540 Oceanography: Physical: Ice mechanics and air/sea/ice exchange processes; 4215 Oceanography: General: Climate and interannual variability (3309); 1640 Global Change: Remote sensing; *KEYWORDS:* ice-atmosphere interactions, ice motion, Antarctic sea ice, remote sensing

Citation: Stammerjohn, S. E., M. R. Drinkwater, R. C. Smith, and X. Liu, Ice-atmosphere interactions during sea-ice advance and retreat in the western Antarctic Peninsula region, *J. Geophys. Res.*, *108*(C10), 3329, doi:10.1029/2002JC001543, 2003.

1. Introduction

[2] Recent satellite remote sensing studies of Arctic and Antarctic sea-ice extent and drift have highlighted the extremely dynamic nature of the polar sea-ice cover, together with characterizing its varied spatial and temporal response to climate forcing. The western Antarctic Peninsula (WAP) region (Figure 1), with its north-south orientation and direct exposure to the prevailing westerlies, in particular appears to be a highly dynamic region that responds rapidly to climate change [e.g., *Smith et al.*, 1999]. West of the peninsula there is a climatic gradient between cold, dry, continental conditions to the south and warm, moist, maritime conditions to the north [*Schwerdtfeger*, 1970; *Sansom*, 1989; *King*, 1994]. Studies show that these contrasting climate regimes can shift in dominance from season-to-season and year-to-year, thus contributing to this region's sensitivity to climate change [*Harangozo et al.*, 1997; *Smith et al.*, 1999]. The WAP region lies within this regional context, and includes specifically the oceanic area extending westward from the Antarctic Peninsula to 80°W and northward to the northern limit of the ice-edge. North of the southern Bellingshausen Sea (Figure 1), there is little sea-ice that persists throughout the summer in the WAP region, and maritime weather prevails here during ice-free months (approximately November to April).

[3] The motivation for this study in part derives from the Palmer Long-Term Ecological Research (Palmer LTER) project (http://pal.lternet.edu), a multidisciplinary program established by the National Science Foundation (NSF) to study the marine ecosystem in the WAP region [*Smith et al.*, 1995; *Ross et al.*, 1996]. The Palmer LTER is finding that the marine ecosystem may be more sensitive to changes in the seasonal timing of sea-ice advance and retreat than to changes in the overall magnitude of winter sea-ice extent [e.g., *Smith et al.*, 1998]. Therefore, in an attempt to better understand what is controlling the temporal evolution of the seasonal sea-ice cover in the WAP region, satellite-derived sea-ice extent, concentration, and drift data are combined with

[1]Department of Earth and Environmental Sciences, Lamont Doherty Earth Observatory of Columbia University, Palisades, New York, USA.
[2]Oceans/Ice Unit (EOP-FSO), European Space Agency (ESTEC), Noordwijk, Netherlands.
[3]Institute for Computational Earth System Science, Santa Barbara, California, USA.
[4]Jet Propulsion Laboratory, California Institute of Technology, Pasadena, California, USA.

0148-0227/03/2002JC001543$09.00

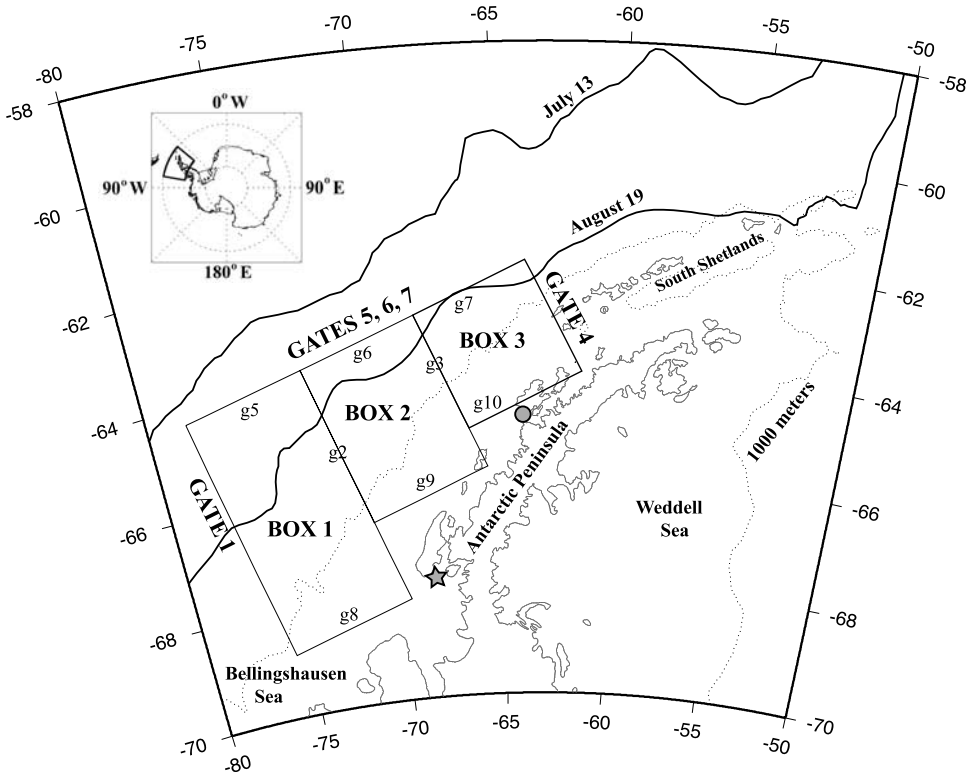

Figure 1. Map of the western Antarctic Peninsula (WAP) region. The WAP region is specifically defined as the oceanic region extending westward from the Antarctic Peninsula to 80°W and northward to the northern limit of the ice-edge. Boxes 1–3 denote the area used in extracting sea-ice extent, concentration, and motion statistics. Collectively, the boxes also include the area studied by the Palmer LTER. The box perimeters comprise the gates used in the volume flux analysis and are labeled accordingly. Weather data were provided by the U.S. Palmer (denoted by circle at 64°46′S, 64°03′W) and the British Antarctic Survey Rothera (denoted by star at 67°34′S, 68°08′W) research stations. Maximum WAP sea-ice extent in 1992 occurred on July 13 and is shown by the northern solid line; the southern solid line is the sea-ice extent approximately 5 weeks later (August 19). The dotted line denotes the 1000-m bathymetric contour.

meteorological data to investigate how the advance and retreat of sea-ice respond to atmospheric forcing. In particular, we address (1) the relative importance of sea-ice dynamics and thermodynamics as they relate to sea-ice extent changes throughout a season and (2) how ice-atmosphere interactions in the WAP region might respond to large-scale atmospheric circulation patterns.

[4] In the following, we first describe the data and methods (section 2), then present the seasonal evolution of the sea-ice drift dynamics in the WAP region for a year (1992) when sea-ice advance and retreat were anomalously early (section 3). To address the larger-scale question, the regional ice-atmosphere interactions in year 1992 are then compared to those in year 1990 when sea-ice advance and retreat were anomalously late. The discussion in section 4 provides a synthesis of previous studies within the context of the 1990 and 1992 comparison and attempts to identify key atmospheric circulation patterns associated with ice-edge anomalies. Conclusions are summarized in section 5.

2. Data and Methods

[5] Our study region is depicted in Figure 1 along with the three boxes used in extracting sea-ice extent, concentration and motion statistics. Sea-ice concentration data are from NASA's Scanning Multichannel Microwave Radiometer (SMMR) and the Defense Meteorological Satellite Program's (DMSP) Special Sensor Microwave/Imager (SSM/I) time series derived from the Bootstrap passive microwave algorithm [*Comiso*, 1995; *Comiso et al.*, 1997]. Sea-ice motion data are derived from SSM/I 85 GHz data and are further described below. The SMMR-SSM/I data were provided by the EOS Distributed Active Archive Center (DAAC) at the National Snow and Ice Data Center, University of Colorado in Boulder, Colorado (http://nsidc.org).

[6] Other satellite data not shown here but that were initially analyzed for higher resolution information and for intersensor comparisons [*Stammerjohn et al.*, 1998] included visible and infrared satellite data from the NOAA Advanced Very High Resolution Radiometer (AVHRR) and the DMSP Operational Linescan System (OLS) sensors, and active microwave satellite data from ERS Synthetic Aperture Radar (SAR) and scatterometer sensors. The AVHRR and OLS data were downlinked by the TeraScan system at Palmer Station (Figure 1), archived at the Antarctic and Arctic Research Center (AARC) at Scripps Institute for Oceanography, and made available by the NSF. The ERS SAR and scatterometer data were made available by the European Space Agency.

[7] The meteorological data include both surface data from Palmer and Rothera Stations (Figure 1) and numerically analyzed data from the National Center for Environmental Prediction/National Center for Atmospheric Research (NCEP/NCAR) Reanalysis Project. Palmer Station weather data were made available through the NSF with the assistance of Antarctic Support Associates. The Rothera Station weather data were made available through the British Antarctic Survey (http://www.antarctica.ac.uk/met/data.html).

[8] The Pathfinder SSM/I sea-ice motion data were supplied by C. Fowler and J. Maslanik of the University of Colorado. Daily gridded sea-ice motion data are generated by tracking features in sequential pairs of SSM/I 85 GHz images. A detailed description of the techniques employed in generating these sea-ice motion products is given by *Maslanik et al.* [1998] and are comparable to data reported by *Kwok et al.* [1998]. Here we use 1-day (24 hour) sea-ice drift vectors generated from sequential daily image pairs, and 5-day means of 1-day motion vectors. The latter were calculated for direct comparison with scatterometer Pathfinder images (see http://www.scp.byu.edu) and to reduce random tracking noise in the daily drift data [*Maslanik et al.*, 1998].

[9] Opening and closing is computed from eight grid point velocities measured around the outer boundary of a 2×2 grid cell area within each box in Figure 1 (grid not shown), consistent with the line-integration methodology of *Stern et al.* [1995]. The opening and closing is calculated by tracing the outer boundary of the 2×2 grid cell area after a 1-day interval has elapsed. The net area difference between the original undeformed (i.e., square) 2×2 grid cell area and the area 1 day later determines whether opening (positive values) or closing (negative values) occurred (a graphical representation of this will be shown in section 3). The net area difference is normalized by the area of the 2×2 grid cells (expressed in units of % d^{-1}), then averaged for the box areas (i.e., boxes 1–3 in Figure 1).

[10] Fluxes were determined for the individual gates shown in Figure 1 and were grouped together to measure net exchanges of sea-ice across each of the critical boundaries around the WAP region (i.e., gate 1: western boundary; gates 5, 6, 7: northern boundary; and gate 4: eastern boundary). Fluxes are estimated by integrating the component of sea-ice velocity orthogonal to the gate transect. The integral is evaluated over the contiguous ice-covered grid points along each designated flux gate in a manner consistent with *Kwok and Rothrock* [1999]. Sea-ice coverage is defined as the gate fraction having a sea-ice concentration exceeding 15% (i.e., is inside the ice edge) and is assumed to be of 100% concentration (due to spatial/temporal variability in the uncertainties of the actual sea-ice concentration retrievals). The volume flux is then determined by multiplying the area flux by an assumed sea-ice thickness distribution. Relatively few sea-ice thickness measurements have been performed in the WAP region [*Smith and Stammerjohn*, 2003], but several studies have been conducted farther to the southwest in the Bellingshausen and Amundsen Sea regions [*Jeffries et al.*, 1994; *Worby et al.*, 1996; *Jeffries et al.*, 1997; *Haas*, 1998]. Although the sea-ice thickness distribution evolves spatially as a function of time, we assume a typical seasonal thickness distribution from the in situ measurements made by *Worby et al.* [1996] in the Bellingshausen Sea at the end of winter. The mean sea-ice thickness and standard deviation in winter were found to be 0.9 and 0.64 m, respectively. These values were chosen over the relatively larger mean (but equivalent standard deviation) of *Haas* [1998] as his values included samples of perennial sea-ice and are therefore biased high, and over the lower mean of *Smith and Stammerjohn* [2003], as their values were from an early winter period that exhibited anomalously low sea-ice extent.

[11] Uncertainties arising in flux estimates are dependent on a number of factors: (1) errors in sea-ice motion tracking, (2) uncertainties in area fluxes though gates, and (3) uncertainties in the assumed sea-ice thickness distribution. In particular, the assumptions of 100% sea-ice concentration and mean thickness become problematic when the ice-edge retreats near the flux gate, because both concentration and thickness often decrease in the marginal ice zone (and drift speeds increase). Thus the volume flux estimates presented here are first-order estimates only and most likely represent an upper bound. We emphasize that this is a first attempt to calculate volume fluxes in this region of Antarctica, and we provide a basic methodology within which new data can be added to improve estimates. Also, we do not directly consider the important contribution of snow-ice [e.g., *Jeffries et al.*, 1994, 1997; *Massom et al.*, 2001] which would have implications for any estimates of fresh water fluxes. To properly estimate fresh water fluxes, more comprehensive sea-ice and snow thickness surveys are required. Once compiled, these could be integrated using the methodology presented here.

[12] It should be noted that we have focused our interest on sea-ice drift changes that were related to wind-forcing. As such we have neglected a potentially important contribution from tidal or inertial forcing, which can contribute to additional deformation and thickening of the sea-ice cover [*Geiger et al.*, 1998; *Padman and Kottmeier*, 2000]. Presently, the temporal resolution of satellite derived sea-ice drift (on the order of 1 day or more) cannot capture the tidal component contributing to sea-ice deformation and/or thickening [*Geiger and Drinkwater*, 2001]. The higher temporal resolution provided by buoys is required, but currently such data are sparse for the WAP region.

[13] Standard error in sea-ice tracking is determined relative to 10 years of Antarctic buoy data originating from the International Program for Antarctic Buoys (IPAB). Comparisons of the SSM/I 85GHz sea-ice drift with IPAB buoy drift data (most of which is concentrated in the Weddell Sea) indicate 1-day RMS errors for x and y component displacements of 0.76 pixels and 0.79 pixels, respectively. A 1-day RMS error of 0.8 pixels is equivalent to about 8 cm/s RMS uncertainty in drift velocity (over a 24-hour interval). Both x and y component RMS errors are smaller in magnitude than the RMS displacement of 1.2 pixels over a daily interval and imply a signal-to-noise ratio of 1.5. Errors have zero mean, are uncorrelated, and have a Gaussian distribution, therefore the RMS value is used as an estimate of the standard tracking error. Daily ice motion estimates are clearly noisy [e.g., *Kwok et al.*, 1998], so we also show 5-day running means of 1-day motion in order to reduce the noise but preserve the real daily variability in motion. Comparisons between the resultant 5-day means

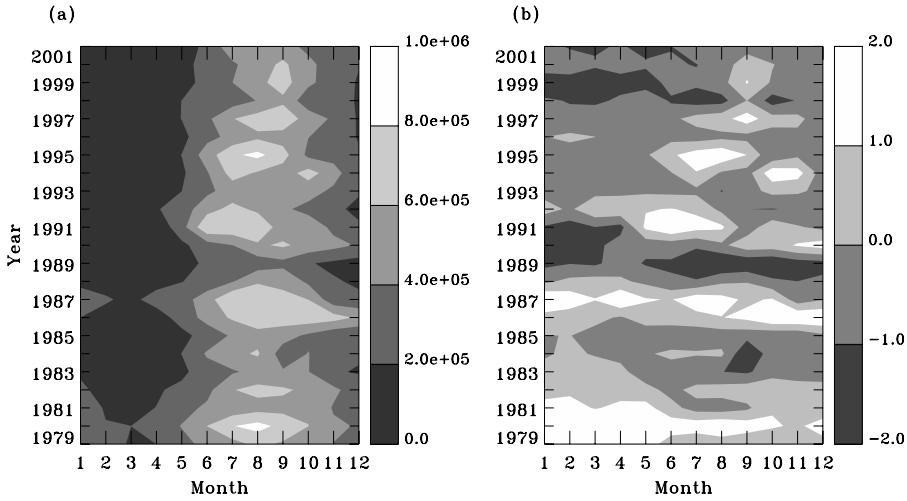

Figure 2. (a) Contour plot of 1979–2001 monthly GSFC Bootstrap SMMR-SSM/I sea-ice extent (km^2) for the WAP region (Figure 1). (b) Contour plot of normalized anomalies (i.e., the monthly anomaly divided by the standard deviation of the monthly mean).

and mean daily buoy motion over the same intervals indicate that the *x* and *y* RMS errors are reduced to 4.7 cm/s and 4.8 cm/s, respectively, with an improved signal-to-noise ratio of 2.6. For a more detailed discussion of sea-ice tracking errors and noise reduction, see *Maslanik et al.* [1998] and *Kwok et al.* [1998].

3. Results

3.1. WAP Sea-Ice Extent

[14] Seasonal and interannual variability of WAP sea-ice is illustrated by a contour plot of monthly SMMR-SSM/I sea-ice extent for the period 1979–2001 (Figure 2a). Annual advance and retreat of sea-ice is viewed from left (January) to right (December) for any given year on the *y* axis. In general, the period of sea-ice advance was either shorter than or equivalent to the period of sea-ice retreat, and the mean months of minimum and maximum sea-ice extent occurred in March and August, respectively [*Stammerjohn and Smith*, 1996]. This mean annual cycle is distinctly different from that observed for most other regions of the Southern Ocean, where the period of advance is longer than the period of retreat, and the minimum and maximum are in February and September, respectively [*Zwally et al.*, 1983; *Gloersen et al.*, 1992].

[15] WAP sea-ice extent during the 1980s showed a marked oscillation between several consecutive years of positive anomalies followed by several consecutive years of negative anomalies (Figure 2b). This several year oscillation agrees with the observations of an Antarctic Circumpolar Wave (ACW) which appears to operate on a 7- to 8-year periodicity [*White and Peterson*, 1996]. However, in the 1990s the persistence in WAP sea-ice anomalies (Figure 2b) broke down (i.e., the anomalies no longer persisted throughout the year, let alone several years), and the 7- to 8-year oscillation was no longer readily apparent [*Smith et al.*, 1996]. In general, the 1990s are marked by more season-to-season variability [*Smith et al.*, 1998].

[16] Despite possible decadal variability, the 21-year record of monthly WAP sea-ice variability is consistently correlated to ENSO behavior [*Smith et al.*, 1996; *Smith and Stammerjohn*, 2001] which also showed higher frequency variability since the 1990s [e.g., *Cullather et al.*, 1996; *Goddard and Graham*, 1997]. This strong ENSO linkage to sea-ice variability appears throughout the South Pacific and western Atlantic sectors of the Southern Ocean [*Harangozo*, 2000; *Yuan and Martinson*, 2000; *Venegas et al.*, 2001; *Yuan and Martinson*, 2001; *Kwok and Comiso*, 2002; *Liu et al.*, 2002], although the nature of the relationship varies longitudinally (and will be discussed further in section 4).

[17] The seasonal variability in the 1990s is illustrated by contrasting the periods of sea-ice advance and retreat for the years 1990 and 1992 (Figure 3). Contrasting the daily and monthly averaged sea-ice extent and open water area for the WAP region emphasizes the synoptic variability revealed by the higher temporal resolution. In comparison to the decade mean (dotted curve), both sea-ice advance and retreat were late in 1990 and early in 1992. Figures 3a and 3c also show that in most cases local maxima in daily sea-ice extent coincided with local maxima in daily open water amount, suggesting that dynamics play a significant role in advancing the ice-edge in this region. In addition, the local open water maxima also may facilitate subsequent rapid retreat events as suggested by *Watkins and Simmonds* [1999].

[18] In the following, we focus in detail on the ice-atmosphere interactions of 1992, when the autumn advance and spring retreat were clearly early. Sea-ice motion and kinematics data for the WAP region during this period were readily available from a previous study characterizing large-scale sea-ice drift in the Weddell Sea in 1992 [*Drinkwater and Liu*, 1999]. At the end of section 3 we then contrast the ice-atmosphere interactions in 1992 against those in 1990 to help distinguish how the WAP region responds to large-scale atmospheric circulation anomalies.

3.2. Sea-Ice Drift During Ice-Edge Advance and Retreat

[19] Previous studies have shown that sea-ice drift is forced predominantly by pressure-gradient winds as determined by the large-scale sea level pressure pattern [*Kwok*

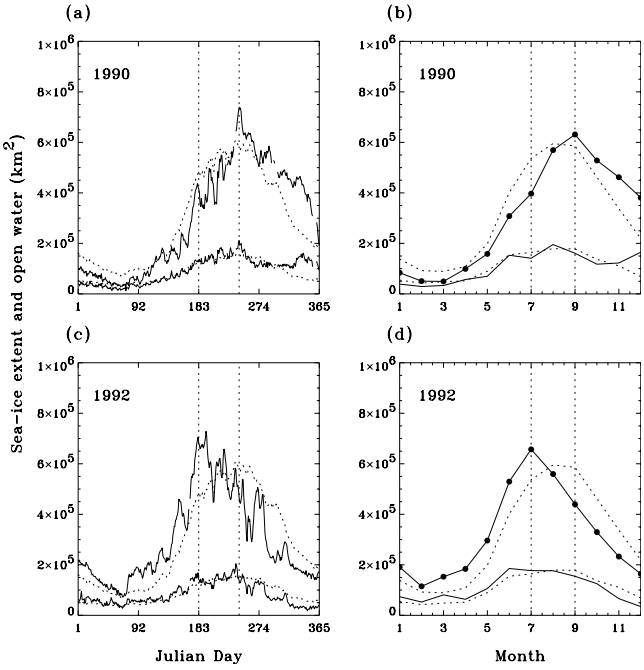

Figure 3. (a, b) 1990 and (c, d) 1992 (left panels) daily and (right panels) monthly averaged GSFC Bootstrap SMMR-SSM/I sea-ice extent (top curves) and open water area (bottom curves) for the WAP region. The dotted curves are the 1990–2000 means, and the dotted vertical lines bracket the July–August winter period.

et al., 1998; *Drinkwater and Liu*, 1999]. It also has been shown that synoptic scale sea-ice drift responds rapidly to changes in wind-forcing on timescales of 12 hours or less (depending on the proximity of the coastline) [*Drinkwater*, 1998]. Away from the coast, sea-ice in the WAP region can drift freely, tracking at approximately 3% of the surface wind speed and 20°–25° to the left of the surface wind direction [*Martinson and Wamser*, 1990]. In general, large-scale sea-ice drift will be more or less aligned with the geostrophic wind, and sea-ice motion vectors will be approximately parallel to isobars of surface pressure [*Drinkwater et al.*, 1999].

[20] A sequence of DMSP SSM/I sea-ice motion images (with NCEP pressure fields overlaid) show daily sea-ice drift and regional atmospheric circulation associated with an increase in sea-ice extent (Figure 4). On days 191 and 192 (Figures 4a–4b) a low-pressure system was located north of the ice-edge in the WAP region which dissipated as a high-pressure system in the southern Bellingshausen Sea intensified on days 193 and 194 (Figures 4c–4d). It is noted, however, that on day 192, the NCEP meteorological analysis misplaced the location of the low pressure center to the west of its actual location. This is inferred by the sea-ice drift, as well as by cloud bands in coincident NOAA AVHRR and DMSP OLS infrared satellite images not shown here. Likewise, the high-pressure center (in the southwestern Bellingshausen Sea) on days 193 and 194 appears to be misplaced to the southwest, again based on the sea-ice drift and coincident infrared images. Similar discrepancies have been observed in intercomparisons of operational products [*Connolley and Harangozo*, 2001], as well as in comparisons of buoy drift data against both ECMWF and NCEP SLP products [*Drinkwater et al.*, 1999].

[21] The time series in Figure 4 show, however, how rapidly sea-ice drift responded to changes in wind-forcing. The southern edge of the low pressure system north of the WAP region on day 191 caused relatively uniform southwestward sea-ice drift. However, as the high-pressure system increased over the southwestern Bellingshausen Sea (on days 192–194), sea-ice drift, in response to the south-southwesterly winds, veered to the north, then northeast, advancing the ice edge. In the northern WAP area (just west of the South Shetland Islands), however, sea-ice drift decelerated with the decrease in winds, resulting in sea-ice compaction and closure of open water areas. The strong north-northeastward sea-ice drift on days 192–194 (Figures 4b–4d) resulted in the notable increase in sea-ice extent observed on those days.

[22] The regional atmospheric circulation and sea-ice drift associated with a decrease in sea-ice extent are shown in Figure 5 for days 204 (Figures 5a–5b) and 205 (Figures 5c–5d). To spatially illustrate how percent opening and closing are derived from daily gridded sea-ice drift (as described in section 2), Figures 5a and 5c show the 1-day deformation grids resulting from the two 24-hour ice drift periods (i.e., for days 204 to 205 and 205 to 206). (Note that the agreement between the NCEP pressure fields and sea-ice drift in Figures 5b and 5d is much better than that shown in Figure 4.) The NCEP sea level pressure fields for day 204 (Figure 5b) show that the ridge of high pressure extending southwards from South America, in combination with the low-pressure system in the southern Bellingshausen Sea, created strong northwesterly winds in the southern WAP region, which compacted the sea-ice cover onshore and effected an ice-edge retreat in that area. The following day (Figures 5c–5d) the wind veered from northwesterly to west-southwesterly with the concurrent dissipation and development of low-pressure systems west and east of the peninsula, respectively. In response, a pulse of fast moving sea-ice was advected from the southwest to the northeast within the WAP region, concurrent with a continued retreat of the ice-edge and compaction of the sea-ice cover onshore. Sea-ice in the northernmost WAP region again decelerated just west of the South Shetland Islands, and consequently significant compression and grid-cell closing took place in that area. The wind-forcing associated with this ice-edge retreat was significantly stronger than that shown for the ice-edge advance in Figure 4.

3.3. Temporal Evolution of an Early Sea-Ice Retreat

[23] The synoptic variability in sea-ice extent, concentration and motion (as depicted in Figures 4 and 5) repeated on a quasi-weekly basis during July–August 1992. Figure 6 shows daily time series of (Figures 6a–6c) weather observations (surface air temperature, sea level pressure, winds), (Figure 6d) sea-ice concentration for boxes 1 (southern) and 3 (northern), and (Figure 6e) sea-ice extent and open water area for the entire WAP region. In the following we will focus on two periods of ice-edge advance (days 184–194 and 206–221) that were each followed by two periods of ice-edge retreat (days 194–206 and 221–232): these four consecutive

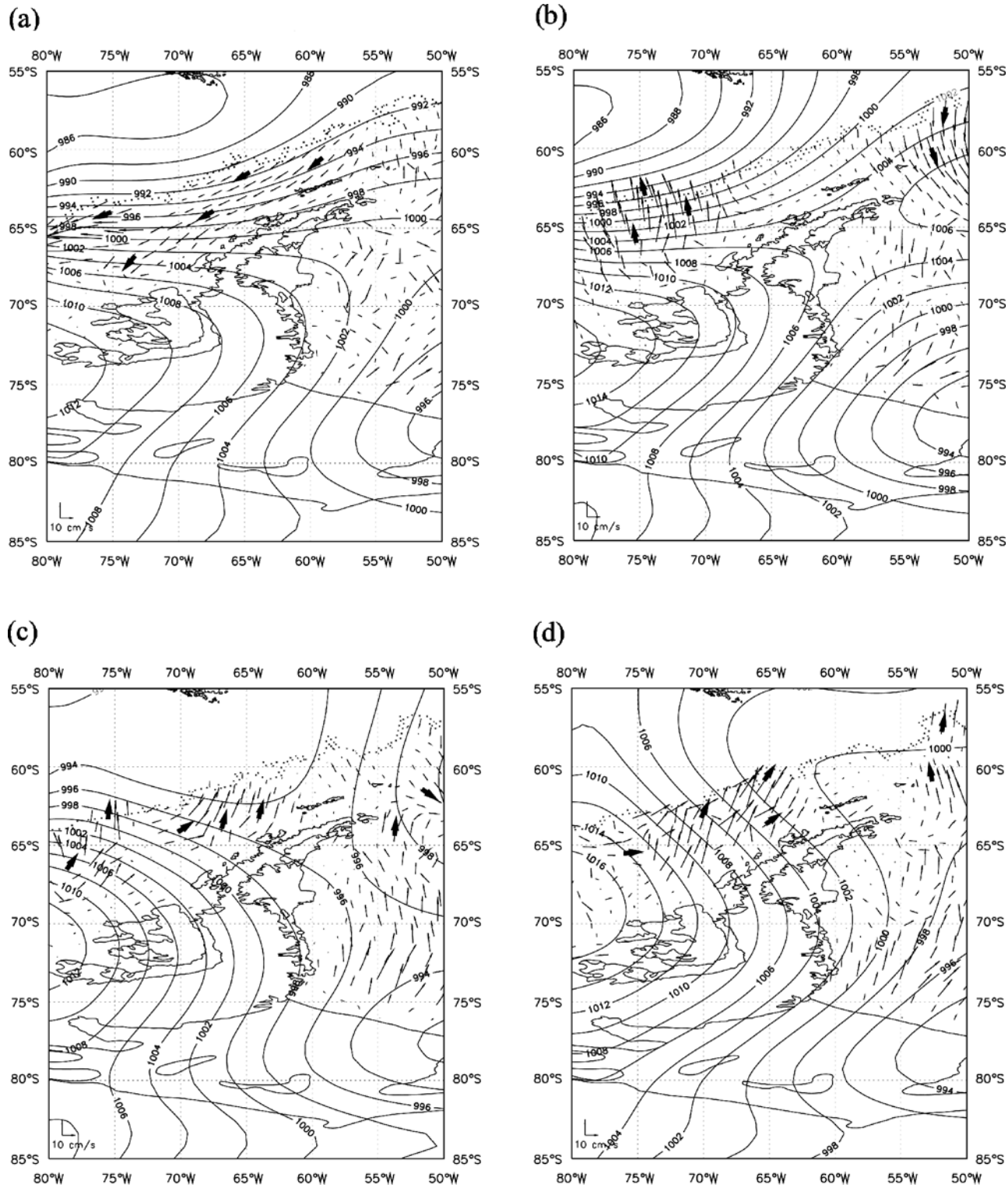

Figure 4. Regional atmospheric circulation and sea-ice drift for days (a) 191, (b) 192, (c) 193, and (d) 194. Sea-ice drift was derived from DMSP SSM/I 85 GHz data, and the sea level pressure fields are from NCEP/NCAR reanalysis data. The larger (overlaid) arrows indicate drift direction only. (See http://pal.lternet.edu/biblio/2003/jgr_ice_atm for full page postscript versions and for contemporaneous DMSP OLS and NOAA AVHRR satellite images.)

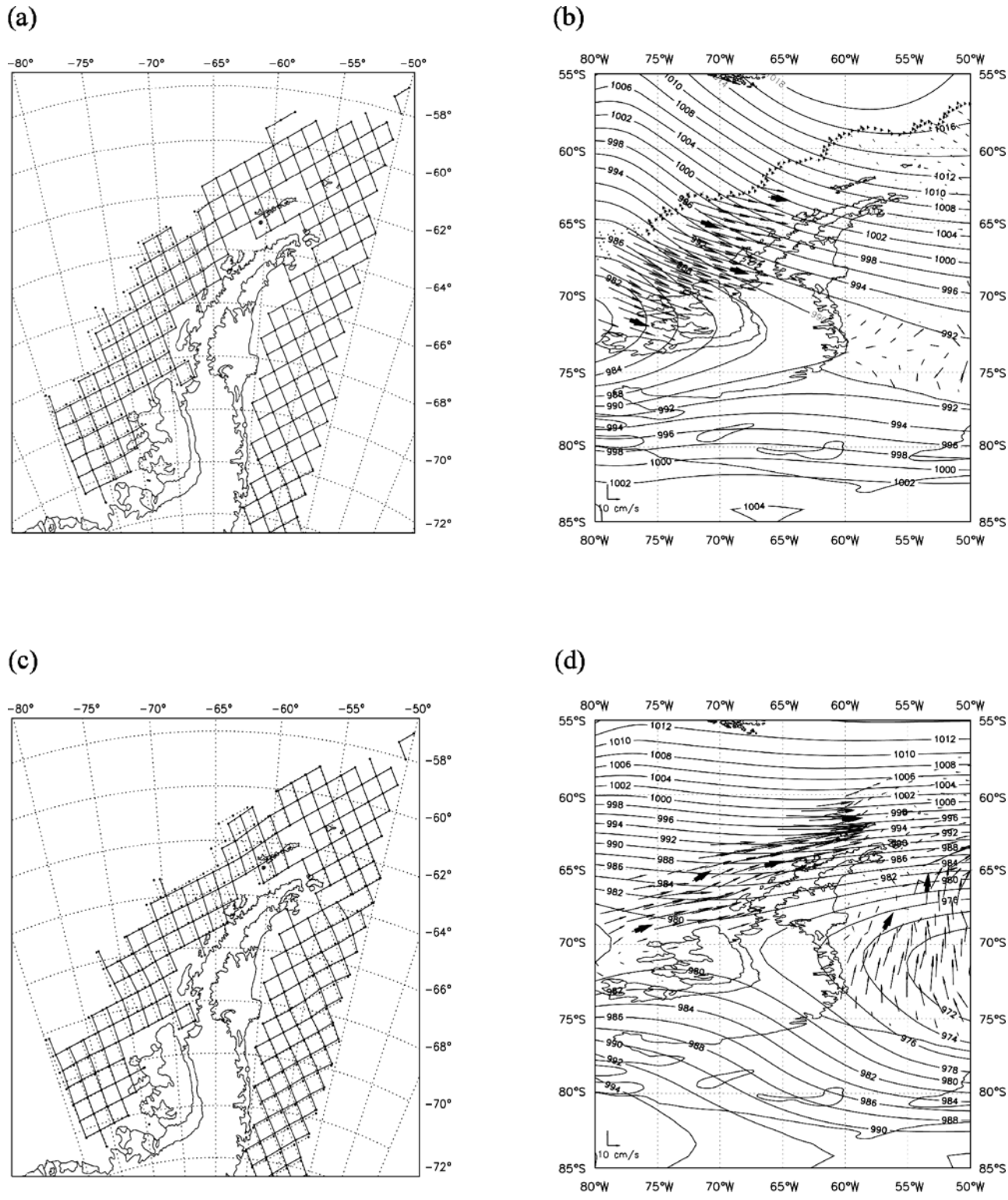

Figure 5. (left panels) DMSP SSM/I 85 GHz derived 1-day deformation grids along with (right panels) the coincident sea-ice drift overlaid with NCEP/NCAR reanalysis sea level pressure fields for days (a, b) 204 and (c, d) 205. The dashed grid lines in Figures 5a and 5c indicate the undeformed Eulerian grid, while the solid grid lines show the deformed grid cells after 24 hours of sea-ice drift. The larger (overlaid) arrows in Figures 5b and 5d indicate drift direction only. (See website quoted in Figure 4 for full page postscript versions of Figures 5b and 5d.)

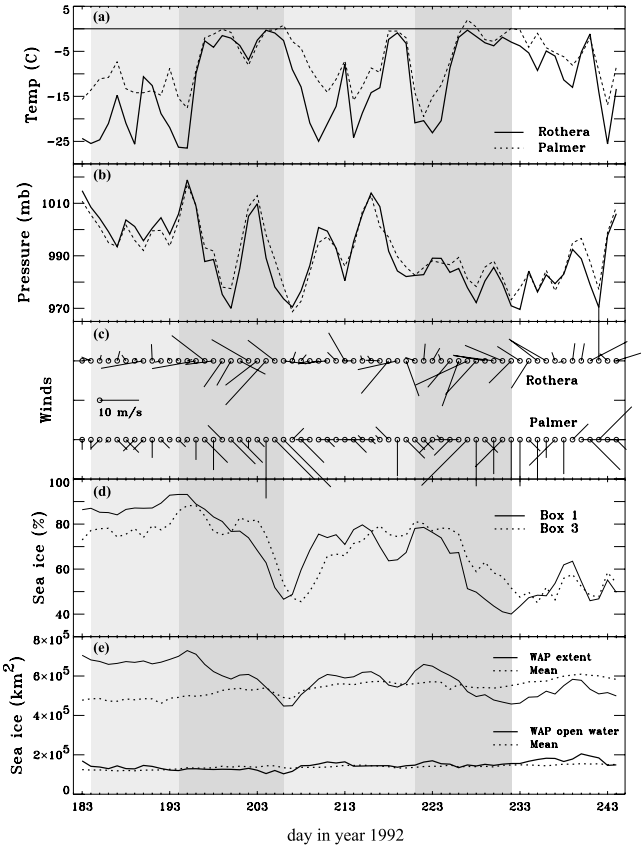

Figure 6. July–August 1992 time series of (a) surface air temperature, (b) sea level pressure, (c) winds, (d) sea-ice concentration within boxes 1 and 3, and (e) sea-ice extent and open water area for the greater WAP region. The weather observations are from Rothera and Palmer Stations, and the sea-ice concentration and extent data are extracted from GSFC Bootstrap SMMR-SSM/I time series data. Vertical shaded panels are periods of ice-edge advance (light shading) and retreat (dark shading).

periods are delineated by the vertical shading. In general, colder air temperatures (usually below −10°C) and light winds (usually less than 5 m/s) occurred during the former periods, while relatively warm air temperatures (usually −5°C to just below 0°C) and strong northerly winds (usually 5 to 15 m/s) occurred during the latter periods. There was a distinct shift from high to low sea level pressure between early July (days 183–195) to early August (day 218 onwards), concurrent with a shift from low to high air temperature. We also note that the local sea-ice extent minima during the two ice-edge retreat periods were below the 1990–2000 mean (see Figure 3). After the second retreat period (i.e., day 232), sea-ice extent remained below the 11-year mean despite short periods of ice-edge advance (accompanied by open water area increases). Thus, by the end of August, the early and rapid spring sea-ice retreat was well underway.

[24] For the four consecutive time periods of ice-edge advance and retreat identified in Figure 6, Figures 7–9 illustrate the associated sea-ice kinematics (where periods of ice-edge advance and retreat are shaded as in Figure 6). Figure 7 shows the July–August 1992 time series of opening (expansion) and closing (contraction) of the sea-ice cover within each of the three boxes (Figures 7a–7c) and for all three boxes combined (Figure 7d). Figures 8 and 9 show volume fluxes through the individual gates and in/out of the three boxes, respectively. Positive volume fluxes indicate net gains or influx of sea-ice, and vice versa for negative fluxes. Recall that the flux calculations are made on the assumption of 100% sea-ice concentration inside the ice-edge; therefore (as noted previously) these estimates are expected to be the upper bound of the volume flux. Finally, because the volume fluxes in and out of boxes 1 and 2 are highly correlated but are different from those in box 3, we refer to the area of boxes 1 and 2 (collectively) as the southern WAP region and of box 3 as the northern WAP region.

[25] The four consecutive periods of ice-edge advance and retreat as seen in Figures 7–9 are summarized as follows. In general, ice-edge advance was associated with an overall expansion of the sea-ice cover and a net export of sea-ice toward the ice-edge (through the northern bound-

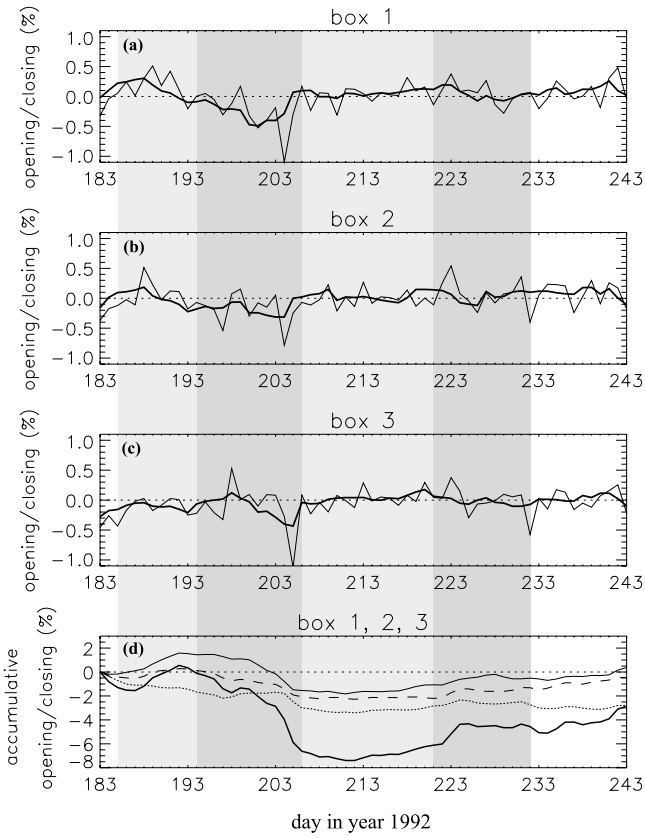

Figure 7. Opening (positive) and closing (negative) of the sea-ice cover in (a) box 1, (b) box 2, and (c) box 3 as daily differences (thin lines) and as 5-day (thick lines) mean daily differences derived from the DMSP SSM/I 85 GHz data. (d) Time-integrated cumulative differences from day 183 onward for box 1 (thin solid line), box 2 (dashed line), box 3 (dotted line), and net change in all boxes (thick solid line). Each curve has been normalized relative to the box area (box 1: ∼132,000 km^2; box 2: ∼87,000 km^2; box 3: ∼65,000 km^2). Vertical shaded panels are periods of ice-edge advance (light shading) and retreat (dark shading).

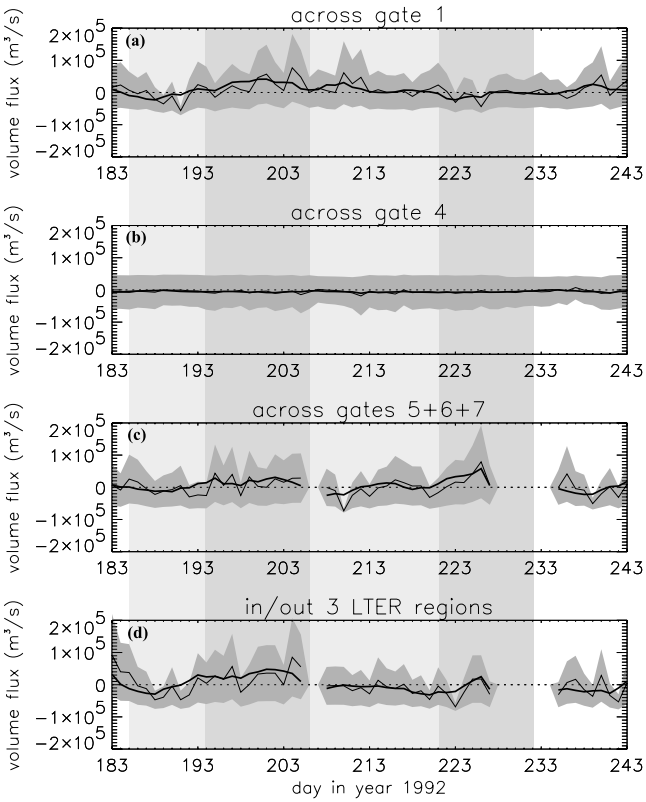

Figure 8. Volume fluxes derived from the DMSP SSM/I 85 GHz data across the gates shown in Figure 1: (a) western boundary (gate 1), (b) eastern boundary (gate 4), and (c) northern boundary (gates 5, 6, 7), together with (d) a summary of net flux in/out of all three boxes combined. A positive volume flux indicates an influx/import of sea-ice, while negative indicates an efflux/export of sea-ice. Daily fluxes are shown by thin lines, and 5-day mean fluxes are shown by thick lines. Error bars (1 sigma) are indicated by the (darkest) shaded region bracketing the curve, and vertical shaded panels are periods of ice-edge advance (light shading) and retreat (dark shading).

ary). However, the first ice-edge advance period (days 184–194) was distinguished by greater opening in the southern WAP region, concurrent with a net export of sea-ice (caused by the expansion) into the southern Bellingshausen Sea (through the western boundary) as well as toward the ice-edge. In contrast, during the second ice-edge advance period (206–221) there was a net import of sea-ice from the southern Bellingshausen Sea, concurrent with a net export of sea-ice toward the ice-edge. Although the winds were typically light at the coastal stations during the ice-edge advance periods, Figure 4 shows that over the pack ice, moderate south-southwesterly winds were associated with sea-ice drift toward the ice-edge.

[26] In general, ice-edge retreat was associated with a net import of sea-ice from the ice-edge (through the northern boundary) and an overall compaction of the sea-ice cover against the peninsula. However, the first ice-edge retreat period (194–206) was distinguished by a net import of sea-ice from the southern Bellingshausen Sea (as well as from the north), which increased over this 12-day period and was punctuated by a large closing event on days 204–205 (see also Figure 5). In contrast, there was a net export of sea-ice into the southern Bellingshausen Sea in the beginning of the second ice-edge retreat period (221–232), concurrent with a net import of sea-ice from the ice-edge associated with opening throughout the sea-ice cover. However, as the net export to the southern Bellingshausen Sea decreased and the net import from the ice-edge increased over this time period, net closing/compaction occurred. As expected, greater export to the southern Bellingshausen Sea occurred with north-northeasterly winds, while greater compaction against the peninsula occurred with west-northwesterly winds.

[27] To summarize the 1992 results, the largest day-to-day changes in sea-ice extent and concentration were related to wind-driven sea-ice drift, the dynamics of which were determined mostly by the meridional component of the atmospheric circulation. The importance of these results is that they directly show the significance of the dynamics, as opposed to thermodynamic processes, in generating ice-edge anomalies. Wind-driven sea-ice drift initiated changes in sea-ice concentration (by divergence/

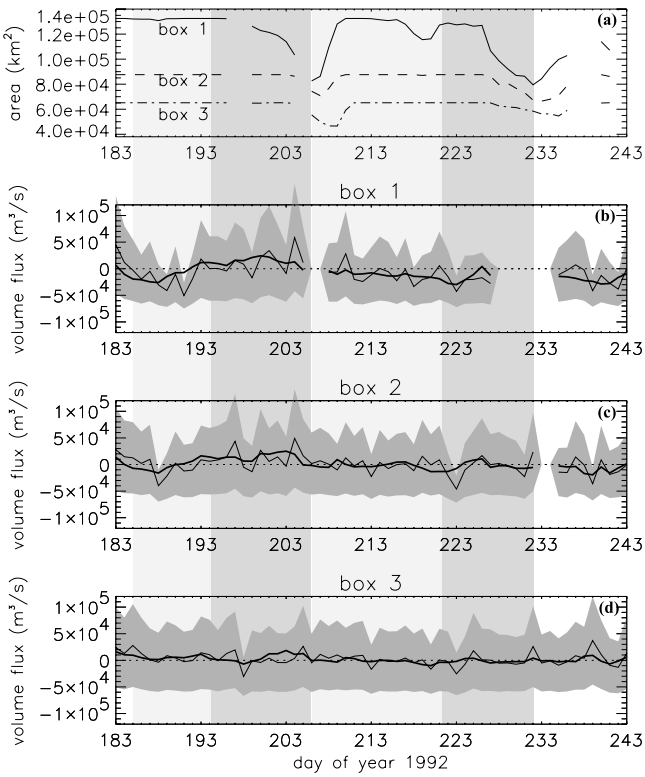

Figure 9. (a) Changes in sea-ice area (km^2) derived from DMSP SSM/I 85 GHz data, in comparison with net volume fluxes (m^3/s) in/out of: (b) box 1, (c) box 2, and (d) box 3. Data gaps in sea-ice area occur when the ice-edge retreats into the box (therefore the box is not completely covered), while data gaps in the net volume fluxes occur when the sides of the box are ice-free (therefore the flux cannot be determined). Daily volume fluxes are shown by thin lines, 5-day mean fluxes are shown by thick lines, and error bars (1 sigma) are indicated by the (darkest) shaded region bracketing the curve. Vertical shaded panels are periods of ice-edge advance (light shading) and retreat (dark shading).

convergence within the pack ice) and in sea-ice extent (by advection of the ice-edge). The winds also advected air temperature anomalies, which in turn were associated with thermodynamic processes involving the growth/ablation of sea-ice. We propose, however, that since the dynamics of sea-ice drift initiated this coupled response, they thereby dominated in the production of ice-edge anomalies. Finally, the persistence and intensity of the meridional wind anomalies throughout the winter season determined the overall timing, duration and magnitude of the annual cycle of sea-ice advance and retreat as affected by sea-ice drift. We next investigate how the wind-driven sea-ice drift dynamics in the WAP region responded to large-scale atmospheric circulation patterns.

3.4. Interannual Variability in Early Versus Late Advance and Retreat

[28] In 1992, the switch from persistently positive to negative ice-edge anomalies was distinctly abrupt, and as mentioned previously, a similar but opposite abrupt mid-winter shift occurred in 1990 (Figure 3). To help identify key atmospheric circulation patterns associated with mid-winter shifts in wind-driven ice-edge anomalies, the regional ice-atmosphere interactions in 1992 are compared to those in 1990. July and August climatologies (1987–1997) of sea level pressure and sea-ice extent and drift are shown in Figures 10a–10b along with the July and August monthly means for 1990 (Figures 10c–10d) and 1992 (Figures 10e–10f).

[29] In general, the sea level pressure contours for 1990 and 1992 show considerably more meridional flow than do the 1987–1997 climatologies (as expected). In particular, the WAP region was dominated by northerly winds (and southward sea-ice drift) in July 1990 (Figure 10c), and the location of the circumpolar trough (CPT), as inferred by the location of the low-pressure system to the west of the Antarctic Peninsula, was very near the ice-edge. The CPT refers to a belt of low sea level pressure, usually located between 60°S–70°S, formed by large numbers of cyclones that have either migrated from midlatitudes or developed within the Antarctic sea-ice or coastal zone [e.g., *Turner et al.*, 1998; *Simmonds and Keay*, 2000]. By the following month (Figure 10d), the CPT had moved south of the ice-edge, and the winds at and north of the ice-edge became zonal, contributing to a late but successful recovery of the sea-ice advance in 1990. These favorable conditions (zonal winds at and north of the ice-edge) were sustained into late spring, during which time sea-ice extent remained well above the 1990–2000 mean (Figure 3).

[30] In contrast to July 1990, July 1992 (Figure 10e) shows a low-pressure system positioned much further west at about 135°W (instead of near 90°W). In further contrast, the WAP region was dominated by high pressure and southerly winds (and northward sea-ice drift). By the following month (Figure 10f), the low-pressure system at 135°W broadened eastward, indicating a strengthening of storm activity in the Amundsen-Bellingshausen Sea regions (and a strengthening of the polar front jet in general). The return of a CPT influence at the ice-edge, accompanied by northerly winds, caused southward sea-ice drift in the southern and central WAP region and an early onset of the sea-ice retreat. These unfavorable conditions (northerly winds at the ice-edge) persisted into late spring, during which time sea-ice extent remained well below the 1990–2000 mean (Figure 3).

[31] Figure 10 shows that the dynamics of sea-ice drift were directly related to the distinctly different regional atmospheric circulation patterns in 1990 versus 1992. These differences raise many questions, the first of which may be what determines the location and strength of the CPT on seasonal time-scales. Numerous studies of Southern Ocean climate variability have explored this question from many different perspectives, and in the discussion that follows, a synthesis of these findings is given within the context of wind-driven sea-ice dynamics and the ice-atmosphere interactions observed in 1990 and 1992.

4. Discussion

[32] Seasonal sea-ice extent anomalies have been linked to the location and strength of the CPT as modulated by the amplitude/phase of the semi-annual oscillation (SAO) and the El Niño-Southern Oscillation (ENSO). For example, previous studies have described the following conditions associated with positive ice-edge anomalies. Locally there is a strengthened SAO [*Harangozo*, 1997; *van den Broeke*, 2000], meaning that the CPT is deepest and farthest poleward in March and September and broadest and farthest equatorward in June and January [e.g., *van Loon*, 1967]. Thus, during mean maximum sea-ice extent (August), the CPT is moving poleward (~70°S) south of the ice-edge. Given this juxtaposition, *Enomoto and Ohmura* [1990] proposed that westerly winds north of the trough promote ice-edge expansion due to northward Ekman forcing, and easterly winds south of the trough promote high sea-ice concentrations near the coast due to southward Ekman forcing. Although *Enomoto and Ohmura* [1990] inferred a dynamical response of sea-ice to regional atmospheric forcing (e.g., that divergence of sea-ice was occurring in the location of the Atmospheric Convergence Line), our results of WAP sea-ice dynamics presented in section 3 directly support their hypothesis: The timing of the semi-annual migration of the CPT dynamically influences the timing of sea-ice advance and retreat via wind-driven sea-ice drift. In other words, dynamic versus thermodynamic processes contributing to sea-ice extent changes can now be distinguished with the relatively recent availability of temporally continuous satellite derived sea-ice drift data.

[33] *Enomoto and Ohmura* [1990] also highlighted the temporal and spatial variability of the SAO-influence on the location of the CPT. They noted that during the time period studied (1982 to 1984), both CPT and sea-ice extent at approximately 90°W (the Bellingshausen Sea sector) behaved quite differently compared to other Southern Ocean regions. The semi-annual fluctuations of the CPT were small, and sea-ice extent at 90°W was often located near the location of the CPT. The implication is that if the ice-edge is in or near this zone of high cyclonic activity, there is a poleward movement of sea-ice ahead of lows (i.e., east of them) and an equatorward movement of sea-ice west of them. Therefore, during a day, no net movement may be visible if the depression is symmetric and fast-moving. However, most depressions in the Antarctic have stronger winds on their west side due to the greater instability of air

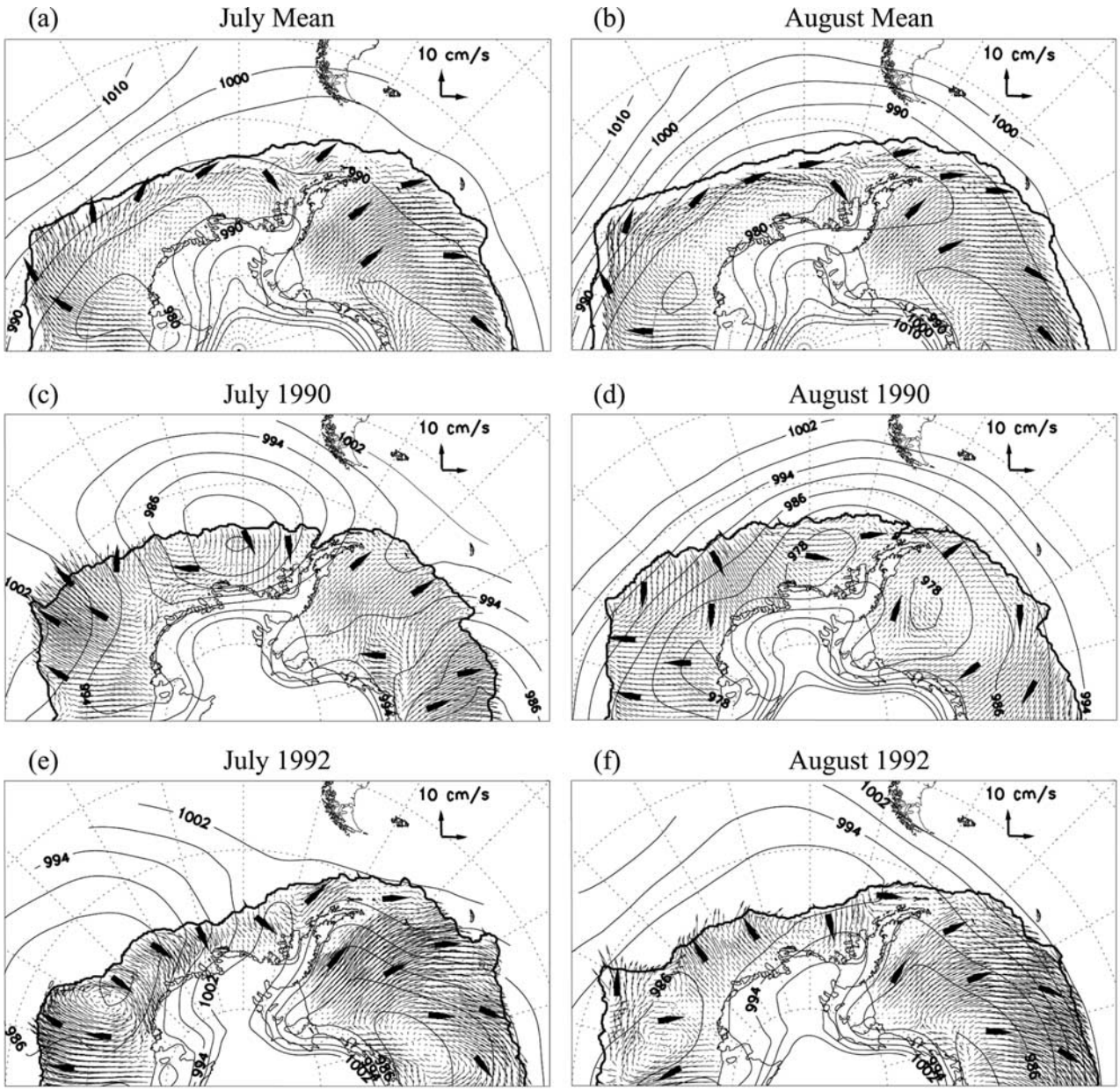

Figure 10. July and August sea level pressure contours and sea-ice drift for the western hemisphere of the Southern Ocean based on (a, b) 1987–1997 means, (c, d) 1990 monthly means, and (e, f) 1992 monthly means. Sea-ice drift was derived from DMSP SSM/I 85 GHz data, and the sea level pressure fields are from NCEP/NCAR reanalysis data. The larger (overlaid) arrows indicate drift direction only. (See website quoted in Figure 4 for full-page postscript versions of each individual panel.)

from the south [*King and Turner*, 1997], thus potentially causing a net movement of sea-ice northward.

[34] In the Bellingshausen Sea, on the other hand, many lows become slow-moving due to the topographic barrier of the peninsula. In this case, warm northerly flow along the eastern limb can effect significant poleward movement of sea-ice along the WAP. Equally important, however, is that the peninsula region also shows in some years a high frequency of persistent blocking [*Sinclair*, 1996; *Renwick*, 1998], in which case the CPT west of the Antarctic Peninsula becomes interrupted, and cold southerly flow prevails along the WAP. Both of these features (the close proximity of the CPT to the sea-ice edge or the high frequency of blocking events) may explain why the WAP region shows strong climate variability and sensitivity [e.g., *Smith et al.*, 1999]. It also may explain why the mean annual cycle in the WAP and greater Bellingshausen Sea differ from that observed for other Southern Ocean regions in that the period of sea-ice retreat can be as long or longer than the period of sea-ice advance [*Stammerjohn and Smith*, 1996].

[35] Studies also have shown that a strengthened SAO in the southeast Pacific is associated with a strengthened subtropical jet (STJ) at 30°S and a weakened polar front

jet (PFJ) at 60°S [*Marshall and King*, 1998]. Consequently, there is a decrease in cyclonic activity in the southeast Pacific region. Also, cold southeast Pacific winters with above average sea-ice extent are associated with El Niño-like conditions [*Harangozo*, 2000; *Yuan and Martinson*, 2000, 2001] which are in turn associated with decreased westerlies in the central Pacific (40°S–55°S) and increased southerlies in the southeast Pacific region [*Garreaud and Battisti*, 1999; *Harangozo*, 2000; *Liu et al.*, 2002; *Carleton*, 2003]. In a similar fashion, conditions associated with negative WAP sea-ice anomalies are essentially the opposite: a weakened SAO, a stationary CPT, a weakened SPJ, a strengthened PFJ, increased westerlies in central Pacific, increased northerlies in the WAP region, and La Niña-like conditions.

[36] The above synthesis is now placed within the context of the sea-ice dynamics observed in the winters of 1990 and 1992, where there was evidence of both a strong and weak SAO-influence occurring at different times during the seasonal sea-ice cycle. The transition in July–August 1990 (Figures 10c–10d) indicated a weakening of the PFJ in association with a strengthening of the STJ in response to tropical Pacific warming. In fact, *Harangozo* [2000] showed a seasonally evolving warming event in 1991 that started in mid-1990. This agrees with high sea-ice extent observed not only in late winter/early spring of 1990 but also in the following autumn/early winter of 1991 (Figure 2). According to *Harangozo* [2000], 1992 was a transition year between a warm and cold ENSO, which agrees with the strengthening of the PFJ seen in the July–August 1992 transition (Figures 10e–10f) and the associated early and rapid sea-ice retreat. Thus the intraseasonal transitions observed in both 1990 and 1992 suggests that the atmospheric circulation in the WAP region responded rapidly to changes in tropical forcing, in addition to associated positive feedbacks within the subpolar region. An example of the latter are the positive air-ocean-ice feedback interactions that can occur near local ice-edge maxima as described by *Yuan et al.* [1999]. Such a positive local feedback may have contributed, for example, to the eastward broadening of the low-pressure system in August 1992 (Figure 10f).

[37] Similar intraseasonal variability in sea-ice anomalies in the eastern South Pacific was observed by *Harangozo* [1994, 1997] for the years 1973–1974 and 1982–1983, although the emphasis in those studies was more on how an SAO-ENSO linkage influenced contrasting longitudinal and interannual variability. More recent studies by *Harangozo* [2000] and others [*Marshall and King*, 1998; *Garreaud and Battisti*, 1999] showed evidence of a higher frequency atmospheric teleconnection between the tropical and South Pacific. This analysis of the wind-driven synoptic variability in sea-ice extent and concentration also suggests a higher frequency atmospheric teleconnection that involves changes in the location and strength of the CPT as modulated by the amplitude/phase of the SAO and ENSO.

[38] It is interesting to note that the increased variability in the timing of sea-ice advance and retreat in the WAP region in the 1990s as compared to the 1980s [*Smith et al.*, 1998] was coincident with a decreasing trend in annual sea-ice extent in the southeast Pacific [*Jacobs and Comiso*, 1997; *Stammerjohn and Smith*, 1997; *Gloersen et al.*, 1999; *Yuan and Martinson*, 2000]. However, the decreasing trend in WAP annual sea-ice extent was mostly due to decreasing trends in spring, summer, and autumn and therefore was manifested not as a decrease in the magnitude of winter sea-ice extent, but as a decrease in the duration of the winter sea-ice extent [*Smith and Stammerjohn*, 2001]. Other studies also have noted, depending on the region, increasing/decreasing trends in the length of the sea-ice season [*Parkinson*, 1994; *Watkins and Simmonds*, 2000]. These regional trends are embedded in an overall increasing trend observed in annual Antarctic sea-ice extent from 1978 to the present [*Cavalieri et al.*, 1997; *Gloersen et al.*, 1999].

[39] The change in the persistence of WAP sea-ice anomalies and the decreasing length of the winter sea-ice season from the 1980s to the 1990s was coincident with an overall weakening of the SAO [*Meehl et al.*, 1998; *Simmonds and Jones*, 1998] and a well-observed increase in storminess in the WAP region [*Turner et al.*, 1997; *King and Harangozo*, 1998; *van den Broeke*, 2000]. *Meehl et al.* [1998] showed that in most years since 1979 the amplitude of the SAO weakened due to a modulation of the temperature gradients between 50°S and 65°S. This modulation appeared to be the result of a warming trend since 1979 that was not evenly distributed throughout the year at each latitude, resulting in a shift in the peaks of the meridional temperature gradient from March and September to May and November. In addition, a seasonal increase in storminess usually occurs during the equinoctial months in association with the SAO. However, *van den Broeke* [2000] showed that, coincident with the overall weakening of the SAO since the late 1970s, storminess increased during solsticial months. This has direct implications for the timing of sea-ice advance and retreat as discussed by *van den Broeke* [2000] and as revealed by the decreasing trend in the length of the WAP winter sea-ice season.

[40] A key to understanding the variability of sea-ice drift dynamics in the southeast Pacific region is to understand what is contributing to the variability of the CPT in the greater South Pacific sector of the Southern Ocean. As described above, the CPT is seasonally influenced by the SAO, and as described by *Simmonds and Jones* [1998] and *Walland and Simmonds* [1999], the SAO shows a consistent relationship between the thermal and pressure fields of the southern extratropics. Thus the mechanism of the SAO (i.e., the meridional temperature gradient between middle and high latitudes) is well described. Therefore the key to understanding the spatial and temporal variability of the CPT in the South Pacific is to understand the variability of the large-scale meridional temperature gradients in the greater Pacific.

[41] Most of the variability in the meridional temperature gradient is related to the El Niño-Southern Oscillation (ENSO), where the response in the western hemisphere of the Southern Ocean is manifested as the Antarctic Dipole (ADP) [*Yuan and Martinson*, 2001]. Also, both observational [*Harangozo*, 2000] and modeling [*Rind et al.*, 2001] studies have shown how changing the SST gradients in the Pacific basin ultimately influences the location and intensity of the CPT and hence the meridional circulation in the southern Pacific. A possible mechanism for this teleconnection is suggested by *Liu et al.* [2002], who analyzed the variability of the regional mean meridional atmospheric circulation as represented by the indirect Ferrel Cell. The

altered storm tracks associated with ENSO variability influence the indirect Ferrel Cell by altering the regions of eddy heat and momentum fluxes, thus shifting the zones of latent heat release and divergence/convergence. Further details of atmospheric teleconnections involving the Southern Ocean are given by *Carleton* [2003].

[42] To summarize our discussion, we have shown that the dynamics of sea-ice drift play a dominant role in the production of sea-ice extent and concentration anomalies in the WAP region, and that these anomalies are tightly coupled to changes in the regional atmospheric circulation. We then attempted to place our 1990 and 1992 ice-atmosphere observations into the broader context of previous findings that have related sea-ice variability to changes in large-scale circumpolar and tropical-polar atmospheric circulation. In particular, we have focused on seasonal variability as affected by changes in the amplitude/phase of the SAO and ENSO. The relationships between sea-ice, SAO, and ENSO are not well understood other than (1) ENSO affects the meridional temperature gradient, (2) the amplitude/phase of the SAO responds to changes in the meridional temperature gradient, and (3) the dynamics of sea-ice drift respond to the regional atmospheric circulation as mediated by the SAO via the meridional temperature gradients. As pointed out by *Meehl et al.* [1998], regional and/or global warming also modulates the meridional temperature gradient. Clearly there are linkages here, but just as clearly there is a need to better understand the details and mechanisms of these linkages. Fortunately, with the increased availability of temporally continuous satellite derived sea-ice drift data, along with insights gained from modeling studies, ongoing research will uncover these details and begin identifying the underlying mechanisms.

5. Conclusions

[43] Sea-ice drift in the WAP region, as in other seasonal sea-ice zones [*Kwok et al.*, 1998; *Drinkwater and Liu*, 1999], is forced predominantly by pressure-gradient winds as determined by large-scale sea level pressure patterns. Strong reversals in drift direction can occur day-to-day, thus advancing or retreating the ice-edge accordingly as observed elsewhere in the Antarctic [*Allison*, 1989; *Massom*, 1992; *Heil and Allison*, 1999]. The important finding of this study is that in the WAP region the dynamics of wind-driven sea-ice drift initiated the coupled dynamical-thermodynamical response involved in sea-ice extent and concentration changes observed in 1992.

[44] The impact of sea-ice drift dynamics on sea-ice fluxes in the WAP region indicated that sea-ice production took place in open water areas created by the relaxation of the sea-ice cover under relatively calm conditions. Such conditions existed mostly in the southern WAP region. When strong northerly winds did occur, however, the impact was pervasive on the entire WAP region and involved compaction of the sea-ice cover against the peninsula, closure of leads, and rafting/ridging of new ice, coincident with large decreases in sea-ice extent. For the study period analyzed, ice-edge advance was accompanied by either sea-ice import from or export to the southern Bellingshausen Sea, and ice-edge retreat was accompanied by either sea-ice export to the southwest or toward the peninsula where it dynamically thickened due to rafting/ridging.

[45] The persistence and intensity of the meridional wind anomalies determined the overall timing, duration and magnitude of the annual cycle of sea-ice advance and retreat as affected by sea-ice drift dynamics. An increase in northerly winds at and north of the ice-edge, associated with a weakened SAO cycle, contributed to the early and rapid sea-ice retreat in the WAP region in mid-July 1992. In contrast, a decrease in northerly winds at and north of the ice-edge, associated with a strengthened SAO cycle, contributed to the late but successful recovery of the sea-ice advance in August 1990. The mid-winter shifts in sea-ice extent anomalies in both 1990 and 1992, coupled with the strong ENSO linkage in the WAP region, suggest that ice-atmosphere interactions in the WAP region respond rapidly to changes in tropical forcing. Further, the decadal variability observed in the persistence of ice-edge anomalies in the WAP region (i.e., the interannual persistence of anomalies in the 1980s versus the increased seasonal variability in the 1990s) may reflect decadal variability in ice-SAO-ENSO interactions, a question being addressed with ongoing research.

[46] Our major findings suggest the following: (1) The dynamics of wind-driven sea-ice drift dominate in the production of ice-edge anomalies, (2) the annual cycle of sea-ice advance and retreat is determined by sea-ice drift via the persistence and intensity of the regional atmospheric circulation, and (3) seasonal changes in the regional atmospheric circulation are associated with changes in the amplitude/phase of the SAO which respond to the meridional temperature gradient as modulated by ENSO and/or regional/global warming. Within this context, we noted that the decreasing trend in annual WAP sea-ice extent in the 1980s and 1990s was due to a decreasing trend in the length (not magnitude) of winter sea-ice extent caused by ice-atmosphere interactions responding to changes in tropical-polar atmospheric circulation anomalies in the Pacific.

[47] As a final note, we emphasize that our study focused mostly on the seasonal variability of sea-ice drift dynamics and did not address the potential role of the atmosphere and/or ocean in maintaining and/or propagating sea-ice anomalies from year-to-year (e.g., the Antarctic Circumpolar Wave) [e.g., *Jacobs and Comiso*, 1997; *Yuan et al.*, 1999; *Gloersen and White*, 2001; *Venegas et al.*, 2001; *Yuan and Martinson*, 2001]. We did show that on seasonal timescales, ice-edge advance can be accompanied by either sea-ice import from or export to the greater Bellingshausen Sea, implying that the greater Bellingshausen Sea may not be a consistent source for ice-edge anomalies in the WAP region. The dominant role that sea-ice drift dynamics plays in the production of ice-edge anomalies, together with a strong intraseasonal ENSO linkage, suggests, however, that sea-ice in the South Pacific sector of the Southern Ocean is capable of quickly and coherently responding to tropical-polar atmospheric circulation anomalies. Thus the appearance of eastward propagating ice-edge anomalies could be the result of coherent adjustments to tropical atmospheric variability.

[48] **Acknowledgments.** R. C. S. and S. E. S. were supported by Radarsat NASA grant NAG5-4126 and by Palmer LTER NSF grant

OPP96-32763. During the revision process, S. E. S. was supported in part by a NASA Fellowship grant NGT5-30391 and a National Ocean and Atmosphere Administration grant/cooperative agreement (NA17RJ1231). M. R. D. and X. L. conducted this research at the Jet Propulsion Laboratory, California Institute of Technology under contract to the National Aeronautics and Space Administration. Funding support was provided by NASA Code YS through RTOP grant 622-82-31. ERS-1 SAR data were provided under ESA Project AO2.USA.129, and the ERS-1 wind scatterometer data were provided by IFREMER as part of ESA Project AO2.USA.119. SIRF Scatterometer images were developed in conjunction with David Long of Brigham Young University, as part of the NASA Scatterometer Climate Record Pathfinder Project. Acknowledgment goes to NCAR for use of the NCEP air pressure re-analysis fields, Chuck Fowler (UCAR) for the SSM/I sea-ice motion fields, and Kirk Ireson (UCSB) for indispensable assistance with the graphics. The views expressed herein are those of the authors and do not necessarily reflect the views of any of the granting agencies or any of its sub-agencies (e.g., NOAA, NASA). Finally, we thank numerous reviewers for their helpful and constructive comments, in particular Hajo Eicken, Rob Massom, Ian Simmonds, and Bruno Tremblay. This is Palmer LTER contribution 233 and LDEO contribution 6527.

References

Allison, I., Pack-ice drift off East Antarctica, *Ann. Glaciol.*, *12*, 1–8, 1989.

Carleton, A. M., Atmospheric teleconnections involving the Southern Ocean, *J. Geophys. Res.*, *108*(C4), 8080, doi:10.1029/2000JC000379, 2003.

Cavalieri, D. J., P. Gloersen, C. L. Parkinson, J. C. Comiso, and H. J. Zwally, Observed hemispheric asymmetry in global sea ice changes, *Science*, *278*, 1104–1106, 1997.

Comiso, J. C., Sea-ice geophysical parameters from SMMR and SSM/I data, in *Oceanographic Applications of Remote Sensing*, edited by M. Ikeda and F. Dobson, pp. 321–338, CRC Press, Boca Raton, Fla., 1995.

Comiso, J. C., D. Cavalieri, C. Parkinson, and P. Gloersen, Passive microwave algorithms for sea ice concentration-A comparison of two techniques, *Remote Sens. Environ.*, *60*(3), 357–384, 1997.

Connolley, W. M., and S. A. Harangozo, A comparison of five numerical weather prediction analysis climatologies in southern high latitudes, *J. Clim.*, *14*, 30–44, 2001.

Cullather, R. I., D. H. Bromwich, and M. L. Van Woert, Interannual variations in Antarctic precipitation related to El Niño Oscillation, *J. Geophys. Res.*, *101*(D14), 19,109–19,118, 1996.

Drinkwater, M. R., Satellite microwave radar observations of Antarctic sea ice, in *Analysis of SAR Data of the Polar Oceans*, edited by C. Tsatsoulis and R. Kwok, pp. 145–187, Springer-Verlag, New York, 1998.

Drinkwater, M. R., and X. Liu, Active and passive microwave determination of the circulation and characteristics of Weddell and Ross sea ice, in *Proceedings of IGARSS'99*, *Rep. 99CH36293*, pp. 314–316, Inst. of Elect. and Elect. Eng., Hamburg, Germany, June 28 to July 2, 1999.

Drinkwater, M. R., R. Kwok, C. A. Geiger, J. A. Maslanik, C. W. Fowler, and W. J. Emery, Quantifying surface fluxes in the ice-covered polar oceans using satellite microwave remote sensing data, paper presented at Ocean Observing System for Climate (OceanObs'99), Ocean Obs. Panel for Clim., San Raphael, France, October 18–22, 1999.

Enomoto, H., and A. Ohmura, Influences of atmospheric half-yearly cycle on the sea ice extent in the Antarctic, *J. Geophys. Res.*, *95*(C6), 9497–9511, 1990.

Garreaud, R. D., and D. S. Battisti, Interannual (ENSO) and interdecadal (ENSO-like) variability in the Southern Hemisphere tropospheric circulation, *J. Clim.*, *12*, 2113–2123, 1999.

Geiger, C. A., and M. R. Drinkwater, The influence of temporal and spatial resolution on sea-ice drift and deformation determination, in *IUTAM Symposium on Scaling Laws in Ice Mechanics and Ice Dynamics*, edited by J. P. Dempsey and H. H. Shen, pp. 407–416, Kluwer Acad., Norwell, Mass., 2001.

Geiger, C. A., S. F. Ackley, and W. D. Hibler, Sea ice drift and deformation processes in the western Weddell Sea, in *Antarctic Sea Ice*: *Physical Processes, Interactions, and Variability*, *Antarct. Res. Ser.*, vol. 74, edited by M. O. Jeffries, pp. 141–160, AGU, Washington, D. C., 1998.

Gloersen, P., and W. B. White, Reestablishing the circumpolar wave in sea ice around Antarctica from one winter to the next, *J. Geophys. Res.*, *106*(C3), 4391–4395, 2001.

Gloersen, P., W. J. Campbell, D. J. Cavalieri, J. C. Comiso, C. L. Parkinson, and H. J. Zwally, *Arctic and Antarctic Sea Ice, 1978–1987*: *Satellite Passive-Microwave Observations and Analysis*, Natl. Aeronaut. and Space Admin., Washington, D. C., 1992.

Gloersen, P., C. L. Parkinson, D. J. Cavalieri, J. C. Comiso, and H. J. Zwally, Spatial distribution of trends and seasonality in the hemispheric sea ice covers: 1978–1996, *J. Geophys. Res.*, *104*(C9), 20,827–20,835, 1999.

Goddard, L., and N. E. Graham, El Niño in the 1990s, *J. Geophys. Res.*, *102*(C5), 10,423–10,436, 1997.

Haas, C., Evaluation of ship-based electromagnetic-inductive thickness measurements of summer sea-ice in the Bellinghausen and Amundsen Seas, Antarctica, *Cold Reg. Sci. Technol.*, *27*, 1–16, 1998.

Harangozo, S. A., Interannual atmospheric circulation-sea ice extent relationships in the Southern Ocean: An analysis for the west Antarctic Peninsula region, paper presented at Sixth Conference on Climate Variations, Am. Meteorol. Soc., Nashville, Tenn., January 23–28 , 1994.

Harangozo, S. A., Atmospheric meridional circulation impacts on contrasting winter sea ice extent in two years in the Pacific sector of the Southern Ocean, *Tellus, Ser. A*, *49*, 388–400, 1997.

Harangozo, S. A., A search for ENSO teleconnections in the west Antarctic Peninsula climate in austral winter, *Int. J. Climatol.*, *20*, 663–679, 2000.

Harangozo, S. A., S. R. Colwell, and J. C. King, An analysis of a 34-year air temperature record from Fossil Bluff (71°S, 68°W), Antarctica, *Antarct. Sci.*, *9*(3), 355–363, 1997.

Heil, P., and I. Allison, The pattern and variability of Antarctic sea-ice drift in the Indian Ocean and western Pacific sectors, *J. Geophys. Res.*, *104*(C7), 15,789–15,802, 1999.

Jacobs, S. S., and J. C. Comiso, Climate variability in the Amundsen and Bellingshausen Seas, *J. Clim.*, *10*, 697–709, 1997.

Jeffries, M. O., R. A. Shaw, K. Morris, A. L. Veazey, and H. R. Krouse, Crystal structure, stable isotopes ($\delta^{18}O$), and development of sea ice in the Ross, Amundsen, and Bellingshausen seas, Antarctica, *J. Geophys. Res.*, *99*(C1), 985–995, 1994.

Jeffries, M. O., A. P. Worby, K. Morris, and W. F. Weeks, Seasonal variations in the properties and structural composition of sea ice and snow cover in the Bellingshausen and Amundsen Seas, Antarctica, *J. Glaciol.*, *43*, 138–151, 1997.

King, J. C., Recent climate variability in the vicinity of the Antarctic Peninsula, *Int. J. Climatol.*, *14*, 357–369, 1994.

King, J. C., and S. A. Harangozo, Climate change in the western Antarctic Peninsula since 1945: Observations and possible causes, *Ann. Glaciol.*, *27*, 571–575, 1998.

King, J. C., and J. Turner, *Antarctic Meteorology and Climatology*, Cambridge Univ. Press, New York, 1997.

Kwok, R., and J. C. Comiso, Southern Ocean climate and sea ice anomalies associated with the Southern Oscillation, *J. Clim.*, *15*, 487–501, 2002.

Kwok, R., and D. A. Rothrock, Variability of Fram Strait ice flux and North Atlantic Oscillation, *J. Geophys. Res.*, *104*(C3), 5177–5189, 1999.

Kwok, R., A. Schweiger, D. A. Rothrock, S. Pang, and C. Kottmeier, Sea ice motion from satellite passive microwave imagery assessed with ERS SAR and buoy motions, *J. Geophys. Res.*, *103*(C4), 8191–8214, 1998.

Liu, J., X. Yuan, D. Rind, and D. G. Martinson, Mechanism study of the ENSO and southern high latitude climate teleconnections, *Geophys. Res. Lett.*, *29*(14), 1679, doi:10.1029/2002GL015143, 2002.

Marshall, G. J., and J. C. King, Southern Hemisphere circulation anomalies associated with extreme Antarctic Peninsula winter temperatures, *Geophys. Res. Lett.*, *25*(13), 2437–2440, 1998.

Martinson, D. G., and C. Wamser, Ice drift and momentum exchange in the winter Antarctic ice pack, *J. Geophys. Res.*, *95*(C2), 1741–1755, 1990.

Maslanik, J., T. Agnew, M. R. Drinkwater, W. Emery, C. Fowler, R. Kwok, and A. Liu, Summary of ice-motion mapping using passive microwave data: Report prepared for the Polar Data Advisory Group, *NASA Spec. Publ.*, *8*, 25 pp., 1998.

Massom, R. A., Observing the advection of sea ice in the Weddell Sea using buoy and satellite passive microwave data, *J. Geophys. Res.*, *97*(C10), 15,559–15,572, 1992.

Massom, R. A., et al., Snow on Antarctic sea ice, *Rev. Geophys.*, *39*(3), 413–445, 2001.

Meehl, G. A., J. W. Hurrell, and H. van Loon, A modulation of the mechanism of the semiannual oscillation in the Southern Hemisphere, *Tellus, Ser. A*, *50*, 442–450, 1998.

Padman, L., and C. Kottmeier, High-frequency ice motion and divergence in the Weddell Sea, *J. Geophys. Res.*, *105*(C2), 3379–3400, 2000.

Parkinson, C. L., Spatial patterns in the length of the sea ice season in the Southern Ocean, *J. Geophys. Res.*, *99*(C8), 16,327–16,339, 1994.

Renwick, J. A., ENSO-related variability in the frequency of South Pacific blocking, *Mon. Weather Rev.*, *126*, 3117–3123, 1998.

Rind, D., M. Chandler, J. Lerner, D. G. Martinson, and X. Yuan, Climate response to basin-specific changes in latitudinal temperature gradients and implications for sea ice variability, *J. Geophys. Res.*, *106*(D17), 20,161–20,173, 2001.

Ross, R. M., E. E. Hofmann, and L. B. Quetin, *Foundations for Ecological Research West of the Antarctic Peninsula*, *Antarct. Res. Ser.*, vol. 70, AGU, Washington, D. C., 1996.

Sansom, J., Antarctic surface temperature time series, *J. Clim.*, *2*(10), 1164–1172, 1989.

Schwerdtfeger, W., The climate of the Antarctic, in *Climates of the Polar Regions*, *World Surv. Climatol.*, vol. 14, edited by S. Orvig, pp. 253–355, Elsevier Sci., New York, 1970.

Simmonds, I., and D. A. Jones, The mean structure and temporal variability of the semiannual oscillation in the southern extratropics, *Int. J. Climatol.*, *18*, 473–504, 1998.

Simmonds, I., and K. Keay, Mean southern hemisphere extratropical cyclone behavior in the 40-year NCEP-NCAR reanalysis, *J. Clim.*, *13*, 873–883, 2000.

Sinclair, M. R., A climatology of anticyclones and blocking for the Southern Hemisphere, *Mon. Weather Rev.*, *124*, 245–263, 1996.

Smith, R. C., and S. E. Stammerjohn, Variations of surface air temperature and sea ice extent in the western Antarctic Peninsula (WAP) region, *Ann. Glaciol.*, *33*, 493–500, 2001.

Smith, R. C., and S. E. Stammerjohn, Palmer LTER: Seasonal process sea ice cruise June–July 1999 (NBP99-06), *Antarct. J. U. S.*, in press, 2003.

Smith, R. C., et al., The Palmer LTER: A long-term ecological research program at Palmer Station, Antarctica, *Oceanography*, *8*(3), 77–86, 1995.

Smith, R. C., S. E. Stammerjohn, and K. S. Baker, Surface air temperature variations in the western Antarctic peninsula region, in *Foundations for Ecological Research West of the Antarctic Peninsula*, *Antarct. Res. Ser.*, vol. 70, edited by R. M. Ross, E. E. Hofmann, and L. B. Quetin, pp. 105–121, AGU, Washington, D. C., 1996.

Smith, R. C., K. S. Baker, and S. E. Stammerjohn, Exploring sea ice indexes for polar ecosystem studies, *BioScience*, *48*(2), 83–93, 1998.

Smith, R. C., et al., Marine ecosystem sensitivity to climate change, *BioScience*, *49*(5), 393–404, 1999.

Stammerjohn, S. E., and R. C. Smith, Spatial and temporal variability of western Antarctic Peninsula sea ice coverage, in *Foundations for Ecological Research West of the Antarctic Peninsula*, *Antarct. Res. Ser.*, vol. 70, edited by R. M. Ross, E. E. Hofmann, and L. B. Quetin, pp. 81–104, AGU, Washington, D. C., 1996.

Stammerjohn, S. E., and R. C. Smith, Opposing Southern Ocean climate patterns as revealed by trends in regional sea ice coverage, *Clim. Change*, *37*(4), 617–639, 1997.

Stammerjohn, S. E., R. C. Smith, M. R. Drinkwater, and X. Liu, Variability in sea-ice coverage and ice-motion dynamics in the PAL LTER study region west of the Antarctic Peninsula, paper presented at 1998 International Geoscience and Remote Sensing Symposium (IGARSS'98), Inst. of Elect. and Elect. Eng., Seattle, Wash., July 6–10 , 1998.

Stern, H. L., D. A. Rothrock, and R. Kwok, Open water production in Arctic sea ice: Satellite measurements and model parameterizations, *J. Geophys. Res.*, *100*(C10), 20,601–20,612, 1995.

Turner, J., S. R. Colwell, and S. Harangozo, Variability of precipitation over the coastal western Antarctic Peninsula from synoptic observations, *J. Geophys. Res.*, *102*(D12), 13,999–14,007, 1997.

Turner, J., G. J. Marshall, and T. A. Lachlan-Cope, Analysis of synoptic-scale low pressure systems within the Antarctic Peninsula sector of the circumpolar trough, *Int. J. Climatol.*, *18*, 253–280, 1998.

van den Broeke, M. R., The semi-annual oscillation and Antarctic Climate: 4. A note on sea ice cover in the Amundsen and Bellingshausen Seas, *Int. J. Climatol.*, *20*, 455–462, 2000.

van Loon, H., The half-yearly oscillations in middle and high southern latitudes and the coreless winter, *J. Atmos. Sci.*, *24*(5), 472–486, 1967.

Venegas, S. A., M. R. Drinkwater, and G. Schaffer, Coupled oscillations in Antarctic sea-ice and atmosphere in the South Pacific sector, *Geophys. Res. Lett.*, *28*(17), 3301–3304, 2001.

Walland, D., and I. Simmonds, Baroclinicity, meridional temperature gradients, and the southern semiannual oscillation, *J. Clim.*, *12*, 3376–3382, 1999.

Watkins, A. B., and I. Simmonds, A late spring surge in the open water of the Antarctic sea ice pack, *Geophys. Res. Lett.*, *26*(10), 1481–1484, 1999.

Watkins, A. B., and I. Simmonds, Current trends in Antarctic sea ice: The 1990s impact on a short climatology, *J. Clim.*, *13*, 4441–4451, 2000.

White, W. B., and R. G. Peterson, An Antarctic circumpolar wave in surface pressure, wind, temperature and sea-ice extent, *Nature*, *380*(6576), 699–702, 1996.

Worby, A. P., M. O. Jeffries, W. F. Weeks, K. Morris, and R. Jaña, The thickness distribution of sea ice and snow cover during late winter in the Bellingshausen and Amundsen Seas, Antarctica, *J. Geophys. Res.*, *101*(C12), 28,441–28,455, 1996.

Yuan, X., and D. G. Martinson, Antarctic sea ice extent variability and its global connectivity, *J. Clim.*, *13*, 1697–1717, 2000.

Yuan, X., and D. G. Martinson, The Antarctic Dipole and its Predictability, *Geophys. Res. Lett.*, *28*(18), 3609–3612, 2001.

Yuan, X., D. G. Martinson, and W. T. Liu, Effect of air-sea-ice interaction on winter 1996 Southern Ocean subpolar storm distribution, *J. Geophys. Res.*, *104*(D2), 1991–2007, 1999.

Zwally, H. J., J. C. Comiso, C. L. Parkinson, W. J. Campbell, F. D. Carsey, and P. Gloersen, *Antarctic Sea Ice, 1973–1976*: *Satellite Passive-Microwave Observations*, Natl. Aeronaut. and Space Admin., Washington, D. C., 1983.

M. R. Drinkwater, Oceans/Ice Unit (EOP-FSO), European Space Agency (ESTEC), 2200 AG Noordwijk ZH, Netherlands. (mark.drinkwater@esa.int)

X. Liu, Jet Propulsion Laboratory, California Institute of Technology, Pasadena, CA 91009, USA. (xiang.liu@jpl.nasa.gov)

R. C. Smith, Institute for Computational Earth System Science, Santa Barbara, CA 93106, USA. (ray@icess.ucsb.edu)

S. E. Stammerjohn, Department of Earth and Environmental Sciences, Lamont Doherty Earth Observatory of Columbia University, Palisades, NY 10964, USA. (sharons@ldeo.columbia.edu)